A protein-trap allele reveals roles for *Drosophila* ATF4 in photoreceptor degeneration, oocyte maturation and wing development

Deepika Vasudevan[1, 2, *], Hidetaka Katow[1], Grace Tang[1], Hyung Don Ryoo[1, *]

[1]Department of Cell Biology, New York University Grossman School of Medicine, New York, NY 10016

[2]Current address: Department of Cell Biology, University of Pittsburgh, Pittsburgh, PA

[*]Corresponding authors: hyungdon.ryoo@nyumc.org

Deepika.vasudevan@pitt.edu

Keywords: ATF4, crc, ER stress, UPR, Retinitis pigmentosa, adRP, retinal degeneration

Abstract

Metazoans have evolved various stress response mechanisms to cope with cellular stress inflicted by external and physiological conditions. The Integrated Stress Response (ISR) is an evolutionarily conserved pathway that mediates adaptation to cellular stress via the transcription factor, ATF4. Loss of function of *Drosophila* ATF4, encoded by the gene *cryptocephal* (*crc*), results in lethality during pupal development. The roles of *crc* in *Drosophila* disease models and adult tissue homeostasis thus remain poorly understood. Here, we report that a protein-trap MiMIC insertion in the *crc* locus generates a crc-GFP fusion protein that allows visualization of crc activity in vivo, and acts as a hypomorphic mutant that uncovers previously unknown roles for *crc*. Specifically, the *crc* protein-trap line shows crc-GFP induction in a *Drosophila* model for Retinitis Pigmentosa (RP). This *crc* allele renders photoreceptors more vulnerable to age-dependent retinal degeneration. *crc* mutant adult animals also show greater susceptibility to amino acid deprivation and reduced levels of known crc transcriptional targets. Furthermore, this mutant allele shows defects in wing veins and oocyte maturation, uncovering previously unknown roles for *crc* in the development of these tissues. Together, our data establish physiological and pathological functions of *crc*-mediated ISR in adult *Drosophila* tissues.

Introduction

Virtually all organisms have evolved stress response mechanisms to mitigate the impact of homeostatic imbalance. The Integrated Stress Response (ISR) pathway, conserved from yeast to humans, is one such mechanism initiated by stress-responsive eIF2α kinases. ISR pathway has been linked to the etiology of a number of human diseases including neurodegenerative disorders, diabetes, and atherosclerosis, amongst others (Chan et al. 2016; Ivanova and Orekhov 2016; Back et al. 2012; Ma et al. 2013). There is thus significant interest in better understanding the ISR signaling pathway.

Each ISR kinase responds to a different type of stress: PERK, an ER-resident kinase, responds to disruption in endoplasmic reticulum (ER) homeostasis (*e.g.* misfolding proteins, calcium flux); GCN2, a cytoplasmic kinase, responds to amino acid deprivation; PKR, a cytoplasmic kinase, responds to double stranded RNA, and; HRI, a cytoplasmic kinase, that responds to oxidative stress (Donnelly et al. 2013). When activated by the corresponding cellular stress, the ISR kinases phosphorylate the same downstream target: the α-subunit of the initiator methionyl-tRNA (Met-tRNA$_i^{Met}$) carrying complex, eIF2. Such phosphorylation of eIF2α kinases leads to decreased availability in Met-tRNA$_i^{Met}$ resulting in lowered cellular translation (Sonenberg and Hinnebusch 2009). However, the translation of some mRNAs with unusual 5' leader arrangements, such as the one encoding the ISR transcription factor ATF4, is induced even under such inhibitory conditions (Hinnebusch et al. 2016). ATF4 is a bZIP (basic Leucine Zipper) transcription factor that induces the expression of stress response genes, including those involved in protein folding chaperones, amino acid transporters, antioxidant genes (Back et al. 2009; Han et al. 2013; Fusakio et al. 2016; Shan et al. 2016).

The number of ISR kinases varies depending on organismal complexity, *e.g.* GCN2 in yeast, GCN2 and PERK in *Caenorhabditis elegans* (worms) and *Drosophila melanogaster* (flies), and all four ISR kinases in *Danio rerio* (zebrafish) and other higher vertebrates (Ryoo 2015; Mitra and Ryoo 2019). ATF4 remains the best-characterized transcription factor that is induced downstream of these kinases (Donnelly et al. 2013), and *Drosophila* has a functionally conserved ortholog referred to as *cryptocephal* (*crc*) (Fristrom 1965; Hewes et al. 2000). In addition to its well-characterized roles during cellular stress, a plethora of studies have demonstrated roles for ISR signaling components during organismal development (Pakos-Zebrucka et al. 2016; Mitra and Ryoo 2019). In *Drosophila*, both *Gcn2* and *Perk* mutants survive to adulthood (Kang et al. 2017; Vasudevan et al. 2020), and the emerging adults show phenotypes in the gut, wings and female ovaries (Wang et al., 2015; Armstrong et al. 2014; Malzer et al. 2018). On the other hand, *crc* mutants fail to reach adulthood (Fristrom 1965; Hewes et al. 2000). The *crc* hypomorphic point mutant, crc^{1}, which causes a single amino acid change, results in delayed larval development and subsequent pupal lethality (Fristrom 1965; Hewes et al. 2000; Vasudevan et al. 2020). The most striking phenotype of the crc^{1} mutants is the failure to evert the adult head during pupariation, along with a failure to elongate their wings and legs (Fristrom 1965; Hewes et al. 2000; Vasudevan et al. 2020; Hewes et al. 2000; Gauthier et al. 2012).

The larval and pupal lethality of known *crc* alleles have however limited our understanding of *crc*'s roles in adult tissues. *crc* is cytogenetically close to the widely used FRT40 element, which has impeded efforts to study this mutation using FRT-mediated mitotic clones. Here, we report that a GFP protein-trap reporter allele in the *crc* locus acts

as a hypomorphic mutant that survives to adulthood. We use this allele to discover that loss of *crc* results in accelerated retinal degeneration in a *Drosophila* model of autosomal dominant retinitis pigmentosa (adRP), a human disease whose etiology is linked to ER stress. Adult *crc* mutants show increased susceptibility to amino acid deprivation, consistent with what was previously known for GCN2. Additionally, we observe several developmental defects in adult tissues, including reduced female fertility due to a block in oogenesis. We also observe wing vein defects and overall reduced wing size in both male and female *crc* mutants.

Results

crc^{GFSTF} is a faithful reporter for endogenous crc levels

In seeking endogenous reporters of crc activity, we examined a "protein trap" line for *crc* generated as part of the Gene Disruption Project (Nagarkar-Jaiswal, DeLuca, et al. 2015; Nagarkar-Jaiswal, Lee, et al. 2015; Venken et al. 2011). The protein trap line is based on a MiMIC (Minos Mediated Integration Cassette) element inserted randomly into various regions in the *Drosophila* genome. The cassette can be subsequently replaced with an EGFP-FlAsH-StrepII-TEV-3xFlag (GFSTF) multi-tag cassette using recombination mediated cassette exchange. One such insertion recovered through this project is in the intronic region of the *Drosophila crc* locus, which has been subsequently replaced with an EGFP-FlAsH-StrepII-TEV-3xFlag (GFSTF) multi-tag cassette using recombination mediated cassette exchange (Fig. 1). The splice donor and acceptor sequences flanking the cassette ensure that the GFSTF multi-tag is incorporated in the coding sequence of most abundantly expressed *crc* splice isoform, *crc-RA* (Hewes et al. 2000), to generate a

multi-tag crc fusion protein (Fig. 1). Henceforth, this *crc* reporter allele is referred to as *crc*^{GFSTF}, with the encoded fusion protein referred to as crc-GFP.

Our lab and others have utilized acute misexpression of Rh1^{G69D}, an ER stress-imposing mutant protein, in third instar larval eye disc tissues using a *GMR-Gal4* driver (*GMR>Rh1*^{G69D}) as a facile method to activate the *Perk-crc* pathway (Ryoo et al. 2007; Kang et al. 2015; Kang et al. 2017). We tested the utility of *crc*^{GFSTF} allele as an endogenous reporter for crc levels, and found robust induction of crc-GFP in third instar larval eye discs specifically in response to misexpression of Rh1^{G69D} protein but not control lacZ protein in the *crc*^{GFSTF}/+ background (Fig. 2a, b). To validate that such induction was downstream of PERK activation by misfolding Rh1^{G69D}, we generated *Perk* mutant FRT clones negatively marked by DsRed expression in the GMR compartment using ey-FLP. While control clones showed no change in the induction of crc-GFP (Fig. 2c), *Perk*^{e01744} mutant clones showed a complete loss of crc-GFP in *GMR>Rh1*^{G69D} eye imaginal discs (Fig. 2d). We also validated these observations in whole animal *Perk*^{e01744} mutants, where we observed a complete loss of crc-GFP in *GMR>Rh1*^{G69D} eye imaginal discs (Fig. S1a, b).

Since the induction of crc in response to PERK activation occurs due to eIF2α phosphorylation (Sonenberg and Hinnebusch 2009), we examined whether crc-GFP induction we observed in Fig. 2a-d similarly occurs through this mechanism. Specifically, we generated a phospho-mimetic transgenic line where the Ser51 in eIF2α is mutated to Asp51 (*UAS-eIF2*α^{S51D}). We also generated a corresponding control transgenic line containing wild type eIF2α (*UAS-eIF2*α^{WT}). We next expressed these transgenes in flies containing *crc*^{GFSTF}. While *GMR>eIF2*α^{WT} discs showed no detectable levels of crc-GFP,

we found that *GMR>eIF2α^{S51D}* led to robust induction of crc-GFP in eye discs as detected by immunostaining with anti-GFP (Fig. 2e, f). These data demonstrate the applicability of *crc^{GFSTF}* as a reliable reporter of endogenous crc expression downstream of ISR activation.

crc^{GFSTF} is a hypomorphic crc mutant allele

Similar to the previously characterized crc hypomorphic mutant allele, *crc^{1}*, we observed that flies homozygous for *crc^{GFSTF}* exhibited a delay in head eversion and showed anterior defects (Fristrom 1965; Hewes et al. 2000). To further assess the effects of the *crc^{GFSTF}* allele, we performed a lethal phase analysis of development starting at the first instar larval stage. We found that a little over 50% of *crc^{GFSTF}* homozygotes were larval lethal (Fig. 3a), which is remarkably similar to larval lethality we previously reported for *crc^{1}* (Vasudevan et al. 2020). However, unlike *crc^{1}* homozygotes, only a small percentage of *crc^{GFSTF}* homozygotes showed prepupal and pupal lethality, with ~30% of animals eclosing as adults (Fig. 3a). To ensure that these developmental defects cannot be attributed to background mutations in the *crc^{GFSTF},* we performed lethal phase analysis on *crc^{GFSTF}* in transheterozygotic combination with the hypomorphic *crc^{1}* allele. We found that *crc^{GFSTF}/crc^{1}* transheterozygotes showed similar levels of larval and pupal lethality to *crc^{GFSTF}* homozygotes, with ~25% of animals surviving to adulthood (Fig. 3a). These data together suggested that the *crc^{GFSTF}* allele may function as a *crc* loss-of-function allele.

To examine if crc transcript levels are affected in *crc^{GFSTF}* mutants, we performed qPCR in the wandering 3rd instar larval stage when crc activity is known to be high in fat tissues (Kang et al. 2015; Kang et al. 2017). We found that *crc^{GFSTF}* homozygotes show

~65% decrease in *crc* transcript levels in comparison to control animals (Fig. 3b). We also tested crc activity by measuring mRNA levels of the well-characterized crc transcriptional target, *4E-BP* (*Drosophila Thor).* We observed ~40% lower levels of *Thor* in crc^{GFSTF} in comparison to control animals (Fig. 3b). This reduction in transcript levels of crc targets was also reproducible crc^{GFSTF}/crc^{1} transheterozygotes (Fig. 3b). Taken together, these data indicate that crc^{GFSTF} acts as a mild hypomorphic mutant allele of *crc*.

crc has a protective role in age-related retinal degeneration and amino acid deprivation

Nearly 30% of all adRP mutations are found in the Rhodopsin gene (Kaushal and Khorana 1994; Illing et al. 2002). Several of these Rhodopsin mutations impose stress in the ER (Kroeger et al. 2019). However, the role of ATF4 in adRP has remained unclear, and we sought to resolve this using the crc^{GFSTF} allele in a *Drosophila* model of adRP.

Clinically, adRP is characterized by age-related loss of peripheral vision, resulting in 'tunnel vision', and night blindness due to degeneration of rod photoreceptors (Kaushal and Khorana 1994). The *Drosophila* genome encodes several Rhodopsin genes, including *ninaE* that encodes the Rhodopsin-1 (Rh1) protein. The $ninaE^{G69D}$ mutation captures essential features of adRP etiology: Flies bearing one copy of the dominant $ninaE^{G69D}$ allele exhibit the age-related retinal degeneration as seen by photoreceptor cell death (Colley et al. 1995; Kurada and O'Tousa 1995). We found that crc^{GFSTF}/crc^{1}; $ninaE^{G69D}$/+ animals exhibited rapid retinal degeneration in comparison to crc^{GFSTF}/+; $ninaE^{G69D}$/+ control animals, as monitored by pseudopupil structures in live flies over a time course of 30 days (Fig. 4a). While the earliest time point when control animals exhibit

retinal degeneration is typically 13-15 days, *crc* homozygous mutant animals exhibited retinal degeneration as early as 2 days, with all animals displaying loss of pseudopupil structures by day 14 (Fig. 4a). Interestingly, we also found that crc^{GFSTF}/crc^{1} animals exhibited age-dependent retinal degeneration even in the absence of $ninaE^{G69D}$, indicating a protective role for crc in photoreceptors under physiological conditions during aging (Fig. 4a).

To measure the expression of crc in aging photoreceptors, we performed western blotting of adult fly heads from young and old (2-week) flies to detect crc-GFP. While young control flies ($crc^{GFSTF}/+$) showed very low levels of crc-GFP, flies bearing one copy of $ninaE^{G69D}$ showed a substantial induction of crc-GFP (Fig. 4b, c). We observed that crc-GFP increases with age in both 2-week old control flies ($crc^{GFSTF}/+$), with a concomitant increase in crc-GFP in $ninaE^{G69D}/+$ flies as well (Fig. 4b, c). These data substantiate the engagement of crc in photoreceptors in response to ER stress inflicted by the ER stress-imposing $Rh1^{G69D}$, thus providing a basis for the protective roles of *Perk* in retinal degeneration.

In addition to rendering a protective effect during ER stress inflicted by $Rh1^{G69D}$, we also tested if crc had an effect during amino acid deprivation in adult animals. We tested this by subjecting crc^{GFSTF}/crc^{1} animals to amino acid deprivation by rearing animals on 5% sucrose-agar. While a majority of control animals survived up to 8 days, crc^{GFSTF}/crc^{1} animals steadily succumbed to amino acid deprivation starting at day 2 with no survivors by day 6 (Fig. 4d). This is consistent with the idea that crc mediates the GCN2 response to amino acid deprivation in adult *Drosophila*.

202 ***crc mutants show wing size and vein defects***

203 *crc*^{GFSTF} provided an opportunity to examine previously unreported roles for *crc* in adult
204 flies. We first observed that wings from both *crc*^{GFSTF} homozygotes and *crc*^{GFSTF}/*crc*^{1}
205 transheterozygotes showed a range of venation defects (Fig. 5a-c). The *Drosophila* wing
206 has five longitudinal veins (annotated L1-L5) and two cross veins, anterior and posterior,
207 ACV and PCV respectively (Fig. 5a). Severe wing defects in *crc*^{GFSTF} homozygous female
208 and male flies were characterized by ectopic venation on L2, between L3 and L4, on L5,
209 and also ectopic cross veins adjacent to the PCV (Fig. 5b, b'). *crc*^{GFSTF}/*crc*^{1}
210 transheterozygotes largely showed milder wing defects, characterized by ectopic
211 venation on the PCV and on L5 (Fig. 5c, c'). We quantified these wing phenotypes in over
212 forty animals of each sex and found that the penetrance and severity of the phenotypes
213 were much stronger in females than in males (Fig. 5d). We also observed that *crc* mutant
214 wings were smaller than in control animals (Fig. 5a-c). Quantification of wing area from
215 animals of each sex revealed a statistically significant decrease in wing blade size in
216 *crc*^{GFSTF} and *crc*^{GFSTF}/*crc*^{1} males and females (Fig. 5e). To exclude the possibility of
217 dominant negative effects of *crc*^{GFSTF}, we also tested wings from *crc*^{GFSTF}/+ heterozygotes
218 but found no wing defects in these animals (Fig. S2). It is notable that *Gcn2* depletion in
219 the wing reportedly causes venation defects (Malzer et al. 2018). Thus, our results
220 suggest that *Gcn2*-mediated crc activation is involved in proper wing vein development.
221

222 ***crc mutants exhibit decreased fertility due to defects in oogenesis***

223 In trying to establish a stock of *crc*^{GFSTF}, we observed that when mated to each other
224 *crc*^{GFSTF} homozygotic males and females produced no viable progeny with very few of the

225 eggs laid hatched to first instar larvae. To determine if this loss of fertility in *crc*^{GFSTF} is
226 due to loss of fertility in males, females or both, we separately mated *crc* mutant females
227 to healthy control (genotype; *yw*) males and vice versa. We observed that while *crc*^{GFSTF}
228 and *crc*^{GFSTF}/*crc*^{1} males produced viable progeny at similar rates to control *yw* males (data
229 not shown), *crc* mutant females showed ~50% reduction in egg laying in comparison to
230 control females (Fig. 6a), again with very few of the eggs laid hatching to first instar larvae.
231 Upon closer observation, we saw defects in the dorsal appendages of eggs laid by *crc*
232 mutant females, with mild phenotypes such as shortening of the appendages to complete
233 absence of one or both appendages (Fig. 6b). These data indicated that the fertility
234 defects in *crc* mutants were due to the loss of crc function in female flies.

235 Dorsal appendages are specified and develop in the final stage of oogenesis. Each
236 *Drosophila* ovary is comprised of 14-16 developing follicles called ovarioles, with germline
237 stem cells residing at the anterior apex undergoing differentiation along the ovariole in
238 individual egg chambers (Lobell et al. 2017). Each egg chamber represents a distinct
239 stage in ovulation, with stage 14 representing a mature egg. To further dissect the dorsal
240 appendage defects, we examined ovaries from *crc* mutant animals. We observed that
241 ovaries from *crc*^{GFSTF} and *crc*^{GFSTF}/*crc*^{1} were considerably swollen in comparison to
242 control ovaries (Fig. S3a). Several ovarioles within *crc* mutant ovaries showed
243 accumulation of stage 10 egg chambers, indicative of an arrest in oogenesis (yellow
244 arrowheads in Fig. S3a). Indeed, examination of individual ovarioles from *crc* mutant
245 ovaries counterstained for actin showed that loss of *crc* results in an abnormal
246 arrangement of early stage egg chambers (Fig. 6c-e). While ovarioles from control
247 animals showed sequentially staged and spaced egg chambers culminating in mature

stage 14 eggs (Fig. 6c), ovarioles from *crc*^{GFSTF} and *crc*^{GFSTF}/*crc*^{1} appeared to be arrested in stage 10, with improper spacing between egg chambers in earlier stages (white arrowheads, Fig. 6d, e). We quantified the number of ovarioles that displayed such arrest and found that more than half of *crc* mutant ovarioles (~9) in each ovary showed stage 10 arrest in comparison to an average of 2-3 ovarioles arrested in ovaries from corresponding control animals (Fig. 6f).

To determine if the arrested egg chambers underwent subsequent cell death, we immunostained ovaries with an antibody that detects proteolytically activated (cleaved) caspase, Dcp-1 (Vasudevan and Ryoo 2016). We observed that stage 10 egg chambers from several *crc*^{GFSTF} and *crc*^{GFSTF}/*crc*^{1} ovarioles showed strong cleaved Dcp-1 staining (Fig. 6g-i). These data strongly suggest that the decrease in fertility in *crc*^{GFSTF} and *crc*^{GFSTF}/*crc*^{1} females is associated with cell death in arrested egg chambers during oogenesis.

To examine which cell types express crc in the ovary, we immunostained ovaries with GFP antibody to detect crc-GFP. However, we were unable to detect crc-GFP in this tissue (Fig. S3b, c), suggesting that crc may regulate ovulation non-autonomously. We also attempted western blotting of ovary extracts to detect crc-GFP but did not observe any detectable signal (data not shown). A previous study had suggested a non-autonomous role for fat body *Gcn2* in the regulation of oogenesis (Armstrong et al. 2014). Consistent with these observations, we were able to detect high levels of crc-GFP fusion protein in adult abdominal fat tissues from *crc*^{GFSTF} animals (Fig. S3d,e). These data raise the possibility that crc mediates Gcn2-signaling in fat tissues to non-autonomously regulate oogenesis.

Discussion

ISR signaling is associated with various pathological conditions, but the role of *Drosophila crc* in adult tissues had remained unclear. This may be in part because the cytogenetic location of *crc* is very close to FRT40, and therefore, attempts to study crc function using conventional genetic mosaics have been unsuccessful. Thus far, our understanding of the role of crc in adult *Drosophila* tissues has entirely relied on RNAi experiments. Loss-of-function mutants, however, allow for unbiased discovery of developmental phenotypes, as is exemplified in our present study where we examined the role of crc in later developmental stages, adult tissues and during aging.

Generally, ER stress-imposing proteins such as $Rh1^{G69D}$ are thought to activate the PERK-mediated ISR response amongst other ER stress responses (Donnelly et al. 2013). It is worth noting here that while both *Drosophila* and mouse models of adRP describe a protective role for *Perk* in retinal degeneration (Chiang et al. 2012; Athanasiou et al. 2017; Vasudevan et al. 2020), there has been conflicting evidence on the role of ATF4 in the mouse adRP model (Bhootada et al. 2016). In this study, we show that loss of *crc* accelerates the age-related retinal degeneration in a *Drosophila* model of adRP. As we have previously shown that *Perk* mutants similarly accelerate retinal degeneration in this model (Vasudevan et al. 2020), we interpret that *crc* mediates the effect of *Perk* in this model. Our data finds that loss of crc renders photoreceptor susceptible to retinal degeneration with age in otherwise wild type animals (solid red line, Fig. 4a). Along with our observation showing an increase in crc protein levels in older flies (Fig. 4b, c), these

data indicate that photoreceptors have physiological stress that requires crc for their survival during aging.

One of the visible phenotypes in adult *crc* mutants is ectopic wing venation (Fig. 5). It has previously been demonstrated that *Gcn2* depletion in the posterior compartment of imaginal discs results in ectopic wing vein formation (Malzer et al. 2010). The study proposed that GCN2 regulates BMP signaling by modulating mRNA translation in wing discs via eIF2α phosphorylation and 4E-BP induction. Our results are consistent with this proposal since 4E-BP is a transcription target of *crc.* In addition, we report here that *crc* loss affects wing size, a finding that has not been reported previously. Given that BMP signaling has also been extensively implicated in determining wing size (Gibson and Perrimon 2005; Shen and Dahmann 2005), it is possible that GCN2-crc signaling regulates wing size via BMP signaling. It is equally possible that GCN2-crc signaling affects tissue size through its role in regulating amino acid transport and metabolism through autonomous and non-autonomous means.

Drosophila fat body is an organ that orchestrates organismal metabolism in response to changes in nutrient availability. While wing development is not known to be sexually dimorphic, fat tissues are known to have sex-specific effects, with particularly profound effects on female fertility is in flies and in all other sexually dimorphic organisms (Valencak et al. 2017). It has been previously demonstrated that loss of *crc* in *Drosophila* larvae leads to reduced fat content and increased starvation susceptibility (Seo et al. 2009). Correlating with this, it had been found that starvation causes effector caspase activation and cell death during mid-oogenesis (McCall 2004; Hou et al., 2008; Jenkins et al., 2013). These observations prompt us to speculate that the caspase-mediated block

316 in oogenesis in *crc* mutants (Fig. 6) may be due to metabolic changes in the female fat
317 body. This hypothesis integrates well with our data showing high crc activity in adult fat
318 tissues (Fig. S3d, e) and observations from a previous study that amino acid sensing by
319 GCN2 in *Drosophila* adult adipocytes regulates germ stem cells in the ovary (Armstrong
320 et al. 2014). However, it remains possible that crc acts autonomously in the ovary but is
321 undetectable using our current methods (Fig. S3b, c).

322 In summary, our study has found utilities for the crc^{GFSTF} allele in discovering a
323 new role for ISR signaling in disease models and during development, and as an
324 endogenous reporter for ISR activation.

325

326 **Methods**

327

328 *Fly husbandry*

329 Flies were reared on cornmeal-molasses media at 25°C under standard conditions except
330 for retinal degeneration experiments when they were reared under constant light. All fly
331 genotypes and sources used in the study are listed in Table S1.

332

333 *Phenotype analysis*

334 Lethal phase analysis was performed as described previously (Vasudevan et al. 2020).
335 Right wings were severed from 1-4 day old flies and imaged using a Nikon SMZ1500
336 microscope outfitted with a Nikon 8MP camera with NIS-Elements software. Wing size
337 was measured using regions of interest (ROI) feature in ImageJ software.

Female fertility was quantified by placing five 1-4 day old virgin females with five *yw* males in a vial containing standard media enhanced with yeast to encourage egg laying. After allowing a day for acclimatization, the flies were moved to a new vial and the number of eggs laid in a 24-hour period were counted and quantified. Eggs were imaged for Fig. 5b by placing them on an apple juice plate and captured with the Nikon SMZ1500 microscope outfitted with 8MP Nikon camera controlled by NIS elements software. Ovaries from female flies in this experiment were dissected in cold PBS and similarly imaged on apple juice plates for Fig. S3a.

qPCR analysis

Total RNA was prepared using TriZol (Invitrogen) from five wandering third instar larva, and cDNA was generated using random hexamers (Fisher Scientific) and Maxima H minus reverse transcriptase (Thermo Fisher) according to manufacturer's protocol. qPCR was performed using PowerSYBR Green Mastermix (Thermo Fisher) using the following primers

crc- Fwd: GGAGTGGCTGTATGACGATAAC

Rev: CATCACTAAGCAACTGGAGAGAA

Thor- Fwd: TAAGATGTCCGCTTCACCCA

Rev: CGTAGATAAGTTTGGTGCCTCC

Rpl15-Fwd: AGGATGCACTTATGGCAAGC

Rev: CCGCAATCCAATACGAGTTC

Immunostaining

Ovaries and fat bodies were dissected in cold PBS from female flies reared for 2-3 days along with *yw* males on standard media enhanced with yeast. Tissues were fixed in 4% PFA in PBT (0.2% Triton-X 100, 1X PBS) for 30 minutes, washed 3x with PBT, and blocked in 1% BSA, PBT for 3 hours, all at room temperature. Tissues were stained overnight at 4°C with the primary antibodies diluted in PBT, following which they were washed 3X with PBT and incubated with AlexaFluor-conjugated secondary antibodies (Invitrogen) in PBT for 3 hours at room temperature. Tissues were mounted in 50% glycerol containing DAPI.

Eye imaginal discs were dissected from wandering 3rd instar larva in cold PBS and fixed in 4% PFA in PBS for 20 minutes, following which they were washed 2x with PBS and permeabilized in 1X PBT for 20 minutes, all at room temperature. Discs were incubated in primary antibodies diluted in PBT for 2 hours, washed 3x in PBT, incubated in AlexaFluor-conjugated secondary antibodies (Invitrogen) in PBT for 1 hour and washed 3x in PBT prior to mounting in 50% glycerol containing DAPI.

Antibodies: Phalloidin-Alexa647 (1:1000, Invitrogen), chicken anti-GFP (1:500, Aves Labs), Rabbit anti-cleaved Dcp-1 (1:100, Cell Signaling), Mouse anti-4C5 for Rh1 (1:500, DSHB), Rabbit anti-eIF2α (1:500, AbCam), rabbit anti-S51 peIF2α (1:500, AbCam).

All images were obtained on a Zeiss LSM 700 confocal microscope with ZEN elements software and a 20X air or 40X water lens.

Retinal degeneration

All experiments were performed in a *white* mutant background since *crc^{GFSTF}*, *crc^{1}*, and *ninaE^{G69D}*, do not have eye color. 0-3 day old male flies were placed (20 animals/vial)

under 1000-lumen light intensity, and their pseudopupil structures monitored under blue light at 3-day intervals for a 30-day period. Media was replaced every 3 days, and flies with disrupted pseudopupils in one or both eyes were marked as having retinal degeneration.

Western blotting

Fly head extracts were prepared from 6 severed male fly heads in 30 μl lysis buffer containing 10mM Tris HCl (pH 7.5), 150mM NaCl, protease inhibitor cocktail (Roche), 1mM EDTA, 1% SDS. Following SDS-PAGE and western blotting, proteins were detected using primary antibodies and IRDye-conjugated secondary antibodies (LI-COR) on the Odyssey system. Primary Rabbit anti-GFP (1:500, Invitrogen) and mouse anti-Tub (1:1000, DHSB).

Amino acid deprivation

0-3 day old female flies were placed (10 animals/vial) in standard media or in vials containing 5% sucrose, 2% agarose prepared in dH_2O. The number of survivors was counted every 24 hours and survivors were moved to new media.

Acknowledgements

We thank Hugo Bellen's laboratory for making available the *crc* MIMIC RMCE line, and Drs. Lacy Barton and Lydia Grmai for discussions on the ovary phenotypes, and Drs. Erika Bach and Jessica Treisman and their laboratories for helpful discussions that improved this work. We thank the Bloomington Drosophila Stock Center (NIH

P40OD018537) for supplying many of the fly stocks, and FlyBase (U41 HG000739) for curating sequence data used in this study.

Contributions

D.V. and H.D.R. conceptualized the project, analyzed the data, and wrote the manuscript. H.K. performed all the wing phenotype analyses, G.T. executed all western blotting experiments, and D.V. performed all other experiments.

Funding

This project was supported by NIH R01 EY020866 and GM125954 to H.D.R., and K99EY029013 to D.V.

Competing Interest

None of the authors have competing interests to disclose.

Bibliography

Armstrong, A.R., Laws, K.M. and Drummond-Barbosa, D. 2014. Adipocyte amino acid sensing controls adult germline stem cell number via the amino acid response pathway and independently of Target of Rapamycin signaling in Drosophila. *Development* 141(23), pp. 4479–4488.

Athanasiou, D., Aguila, M., Bellingham, J., Kanuga, N., Adamson, P. and Cheetham, M.E. 2017. The role of the ER stress-response protein PERK in rhodopsin retinitis pigmentosa. *Human Molecular Genetics* 26(24), pp. 4896–4905.

Back, S.H., Kang, S.-W., Han, J. and Chung, H.-T. 2012. Endoplasmic reticulum stress in the β-cell pathogenesis of type 2 diabetes. *Experimental diabetes research* 2012, p. 618396.

Back, S.H., Scheuner, D., Han, J., et al. 2009. Translation attenuation through eIF2alpha phosphorylation prevents oxidative stress and maintains the differentiated state in beta cells. *Cell Metabolism* 10(1), pp. 13–26.

Bhootada, Y., Kotla, P., Zolotukhin, S., et al. 2016. Limited ATF4 Expression in Degenerating Retinas with Ongoing ER Stress Promotes Photoreceptor Survival in a Mouse Model of Autosomal Dominant Retinitis Pigmentosa. *Plos One* 11(5), p. e0154779.

Chan, P., Stolz, J., Kohl, S., Chiang, W.-C. and Lin, J.H. 2016. Endoplasmic reticulum stress in human photoreceptor diseases. *Brain Research* 1648, pp. 538–541.

Chiang, W.-C., Hiramatsu, N., Messah, C., Kroeger, H. and Lin, J.H. 2012. Selective activation of ATF6 and PERK endoplasmic reticulum stress signaling pathways prevent

445 mutant rhodopsin accumulation. *Investigative Ophthalmology & Visual Science* 53(11),
446 pp. 7159–7166.
447 Colley, N.J., Cassill, J.A., Baker, E.K. and Zuker, C.S. 1995. Defective intracellular
448 transport is the molecular basis of rhodopsin-dependent dominant retinal degeneration.
449 *Proceedings of the National Academy of Sciences of the United States of America*
450 92(7), pp. 3070–3074.
451 Donnelly, N., Gorman, A.M., Gupta, S. and Samali, A. 2013. The eIF2α kinases: their
452 structures and functions. *Cellular and Molecular Life Sciences* 70(19), pp. 3493–3511.
453 Fristrom, J.W. 1965. Development of the morphological mutant cryptocephal of
454 Drosophila melanogaster. *Genetics* 52(2), pp. 297–318.
455 Fusakio, M.E., Willy, J.A., Wang, Y., et al. 2016. Transcription factor ATF4 directs basal
456 and stress-induced gene expression in the unfolded protein response and cholesterol
457 metabolism in the liver. *Molecular Biology of the Cell* 27(9), pp. 1536–1551.
458 Gauthier, S.A., VanHaaften, E., Cherbas, L., Cherbas, P. and Hewes, R.S. 2012.
459 Cryptocephal, the Drosophila melanogaster ATF4, is a specific coactivator for ecdysone
460 receptor isoform B2. *PLoS Genetics* 8(8), p. e1002883.
461 Gibson, M.C. and Perrimon, N. 2005. Extrusion and death of DPP/BMP-compromised
462 epithelial cells in the developing Drosophila wing. *Science* 307(5716), pp. 1785–1789.
463 Han, J., Back, S.H., Hur, J., et al. 2013. ER-stress-induced transcriptional regulation
464 increases protein synthesis leading to cell death. *Nature Cell Biology* 15(5), pp. 481–
465 490.
466 Hewes, R.S., Schaefer, A.M. and Taghert, P.H. 2000. The cryptocephal gene (ATF4)
467 encodes multiple basic-leucine zipper proteins controlling molting and metamorphosis in

Drosophila. *Genetics* 155(4), pp. 1711–1723.

Hinnebusch, A.G., Ivanov, I.P. and Sonenberg, N. 2016. Translational control by 5'-untranslated regions of eukaryotic mRNAs. *Science* 352(6292), pp. 1413–1416.

Hou, Y.C.C., Chittaranjan, S., Barbosa, S.G., McCall, K., Gorski, S.M. 2008. Effector caspase Dcp-1 and IAP protein Bruce regulate starvation-induced autophagy during Drosophila melanogaster oogenesis. *J. Cell Biol.* 182(6), pp. 1127-1139.

Illing, M.E., Rajan, R.S., Bence, N.F. and Kopito, R.R. 2002. A rhodopsin mutant linked to autosomal dominant retinitis pigmentosa is prone to aggregate and interacts with the ubiquitin proteasome system. *The Journal of Biological Chemistry* 277(37), pp. 34150–34160.

Ivanova, E.A. and Orekhov, A.N. 2016. The role of endoplasmic reticulum stress and unfolded protein response in atherosclerosis. *International Journal of Molecular Sciences* 17(2).

Jenkins, V.K., Timmons, A.K., McCall, K. 2013. Diversity of cell death pathways: insight from the fly ovary. *Trends Cell Biol.* 23(11), pp 567-574.

Kang, K., Ryoo, H.D., Park, J.-E., Yoon, J.-H. and Kang, M.-J. 2015. A Drosophila Reporter for the Translational Activation of ATF4 Marks Stressed Cells during Development. *Plos One* 10(5), p. e0126795.

Kang, M.-J. and Ryoo, H.D. 2009. Suppression of retinal degeneration in Drosophila by stimulation of ER-associated degradation. *Proceedings of the National Academy of Sciences of the United States of America* 106(40), pp. 17043–17048.

Kang, M.-J., Vasudevan, D., Kang, K., et al. 2017. 4E-BP is a target of the GCN2-ATF4 pathway during Drosophila development and aging. *The Journal of Cell Biology* 216(1),

pp. 115–129.

Kaushal, S. and Khorana, H.G. 1994. Structure and function in rhodopsin. 7. Point mutations associated with autosomal dominant retinitis pigmentosa. *Biochemistry* 33(20), pp. 6121–6128.

Kroeger, H., Chiang, W.-C., Felden, J., Nguyen, A. and Lin, J.H. 2019. ER stress and unfolded protein response in ocular health and disease. *The FEBS Journal* 286(2), pp. 399–412.

Kurada, P. and O'Tousa, J.E. 1995. Retinal degeneration caused by dominant rhodopsin mutations in Drosophila. *Neuron* 14(3), pp. 571–579.

Lobell, A.S., Kaspari, R.R., Serrano Negron, Y.L. and Harbison, S.T. 2017. The Genetic Architecture of Ovariole Number in Drosophila melanogaster: Genes with Major, Quantitative, and Pleiotropic Effects. *G3 (Bethesda, Md.)* 7(7), pp. 2391–2403.

Ma, T., Trinh, M.A., Wexler, A.J., et al. 2013. Suppression of eIF2α kinases alleviates Alzheimer's disease-related plasticity and memory deficits. *Nature Neuroscience* 16(9), pp. 1299–1305.

Malzer, E., Daly, M.-L., Moloney, A., et al. 2010. Impaired tissue growth is mediated by checkpoint kinase 1 (CHK1) in the integrated stress response. *Journal of Cell Science* 123(Pt 17), pp. 2892–2900.

Malzer, E., Dominicus, C.S., Chambers, J.E., Dickens, J.A., Mookerjee, S. and Marciniak, S.J. 2018. The integrated stress response regulates BMP signalling through effects on translation. *BMC Biology* 16(1), p. 34.

McCall, K. 2004. Eggs over easy: cell death in the Drosophila ovary. *Dev. Biol.* 274(1), p. 3-14.

514 Mitra, S. and Ryoo, H.D. 2019. The unfolded protein response in metazoan
515 development. *Journal of Cell Science* 132(5).
516 Nagarkar-Jaiswal, S., DeLuca, S.Z., Lee, P.-T., et al. 2015. A genetic toolkit for tagging
517 intronic MiMIC containing genes. *eLife* 4.
518 Nagarkar-Jaiswal, S., Lee, P.-T., Campbell, M.E., et al. 2015. A library of MiMICs allows
519 tagging of genes and reversible, spatial and temporal knockdown of proteins in
520 Drosophila. *eLife* 4.
521 Pakos-Zebrucka, K., Koryga, I., Mnich, K., Ljujic, M., Samali, A. and Gorman, A.M.
522 2016. The integrated stress response. *EMBO Reports* 17(10), pp. 1374–1395.
523 Ryoo, H.D. 2015. Drosophila as a model for unfolded protein response research. *BMB*
524 *Reports* 48(8), pp. 445–453.
525 Ryoo, H.D., Domingos, P.M., Kang, M.-J. and Steller, H. 2007. Unfolded protein
526 response in a Drosophila model for retinal degeneration. *The EMBO Journal* 26(1), pp.
527 242–252.
528 Seo, J., Fortuno, E.S., Suh, J.M., et al. 2009. Atf4 regulates obesity, glucose
529 homeostasis, and energy expenditure. *Diabetes* 58(11), pp. 2565–2573.
530 Shan, J., Zhang, F., Sharkey, J., Tang, T.A., Örd, T. and Kilberg, M.S. 2016. The C/ebp-
531 Atf response element (CARE) location reveals two distinct Atf4-dependent, elongation-
532 mediated mechanisms for transcriptional induction of aminoacyl-tRNA synthetase genes
533 in response to amino acid limitation. *Nucleic Acids Research* 44(20), pp. 9719–9732.
534 Shen, J. and Dahmann, C. 2005. Extrusion of cells with inappropriate Dpp signaling
535 from Drosophila wing disc epithelia. *Science* 307(5716), pp. 1789–1790.
536 Sonenberg, N. and Hinnebusch, A.G. 2009. Regulation of translation initiation in

537 eukaryotes: mechanisms and biological targets. *Cell* 136(4), pp. 731–745.
538 Valencak, T.G., Osterrieder, A. and Schulz, T.J. 2017. Sex matters: The effects of
539 biological sex on adipose tissue biology and energy metabolism. *Redox biology* 12, pp.
540 806–813.
541 Vasudevan, D., Clark, N.K., Sam, J., et al. 2017. The GCN2-ATF4 Signaling Pathway
542 Induces 4E-BP to Bias Translation and Boost Antimicrobial Peptide Synthesis in
543 Response to Bacterial Infection. *Cell reports* 21(8), pp. 2039–2047.
544 Vasudevan, D., Neuman, S.D., Yang, A., et al. 2020. Translational induction of ATF4
545 during integrated stress response requires noncanonical initiation factors eIF2D and
546 DENR. *Nature Communications* 11(1), p. 4677.
547 Vasudevan, D. and Ryoo, H.D. 2016. Detection of cell death in drosophila tissues.
548 *Methods in Molecular Biology* 1419, pp. 131–144.
549 Venken, K.J.T., Schulze, K.L., Haelterman, N.A., et al. 2011. MiMIC: a highly versatile
550 transposon insertion resource for engineering Drosophila melanogaster genes. *Nature*
551 *Methods* 8(9), pp. 737–743.
552 Wang, L., Ryoo, H.D., Qi, Y. and Jasper, H. 2015. PERK limits drosophila lifespan by
553 promoting intestinal stem cell proliferation in response to ER stress. *PLoS Genetics*
554 11(5), p. e1005220.
555
556

557 **Figures**

Figure 1

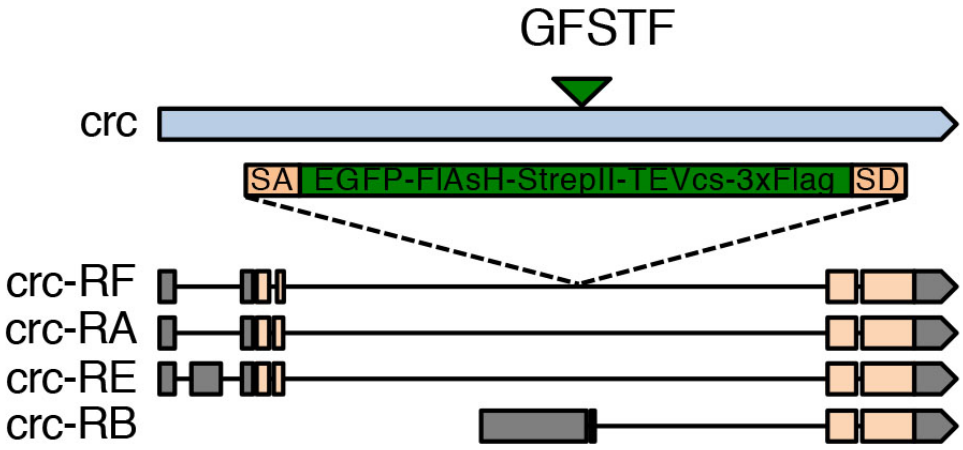

558

559 **Fig. 1. Schematic of the *crc* cytogenetic locus**

560 The *crc* gene (blue bar) is known to encode at least four splice variants *crc-RA*, *-RB*, *-RE*,
561 and *–RF.* These splice isoforms vary in their 5' leader sequences (gray bars) and their
562 coding exons (beige bars). MiMIC-mediated insertion of the GFSTF cassette in the
563 genomic locus (green triangle) with a splice acceptor (SA) and splice donor (SD)
564 sequences predicts the inclusion of a multi-tag exon (green box) in all the *crc* isoforms
565 except *crc-RB*.

566

567

Figure 2

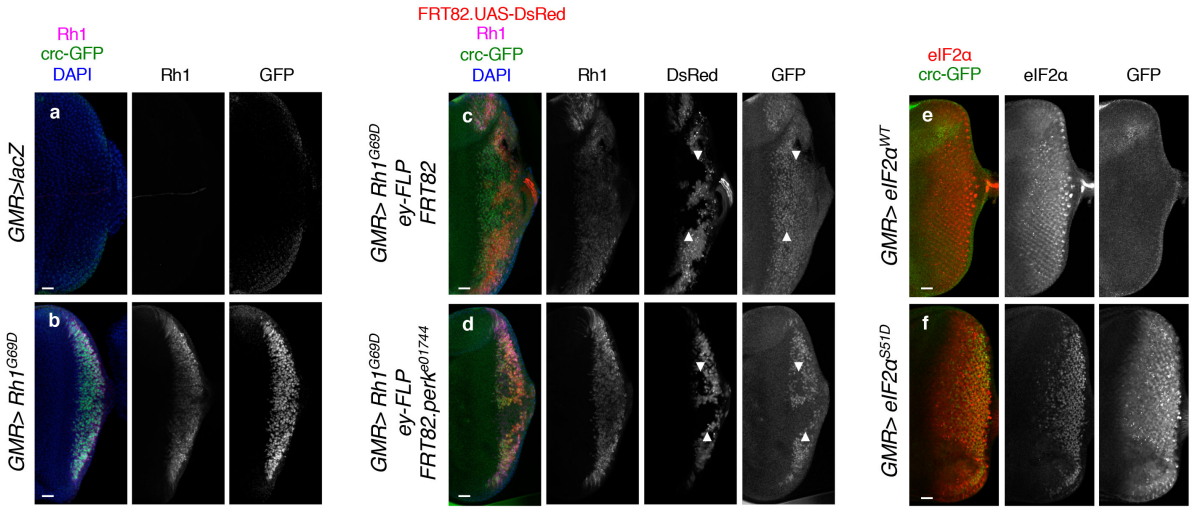

Fig. 2. ***crc*^{GFSTF} is a reporter for crc activity in vivo**

a-b. Confocal images from eye imaginal discs from wandering third instar larva where *GMR-Gal4* drives the expression of either a control protein (*GMR>lacZ*) or mutant Rh1 (*GMR>Rh1*^{G69D}), in the *crc*^{GFSTF}/+ background. Here and in following images, the crc-GFP fusion protein was detected with anti-GFP (green), Rh1 was detected with 4C5 antibody (magenta), DAPI (blue) stains the nucleus. Rh1 and GFP single channels are shown separately in black and white; anterior is the left, posterior to the right; scale bars represent 25 μM.

c-d. Confocal images of eye imaginal discs misexpressing Rh1^{G69D} (*GMR>Rh1*^{G69D}) showing control clones (c, FRT82) and *Perk* mutant clones (d, *FRT82.perk*^{e01744}) generated by eyeless-flippase (*ey-FLP*) in the *crc*^{GFSTF}/+ background. Clones are negatively marked with DsRed (red). This DsRed expression was also driven by *GMR>* (white arrowheads). Rh1, DsRed and GFP single channels are separately shown in black and white images. The absence of GFP in DsRed negative clones demonstrate the effect of loss of *Perk* on crc-GFP induction in response to Rh1^{G69D}.

584 e-f. Confocal images of eye imaginal discs showing crc-GFP expression in response to
585 wildtype eIF2α (*eIF2α*^{WT}) or phospho-mimetic eIF2α (*eIF2α*^{S51D}) ectopically expressed
586 with *GMR-Gal4* (*GMR>*). Ectopic expression was confirmed by staining with anti-eIF2α
587 (red). eIF2α and GFP single channels are shown in black and white.
588
589

Figure 3

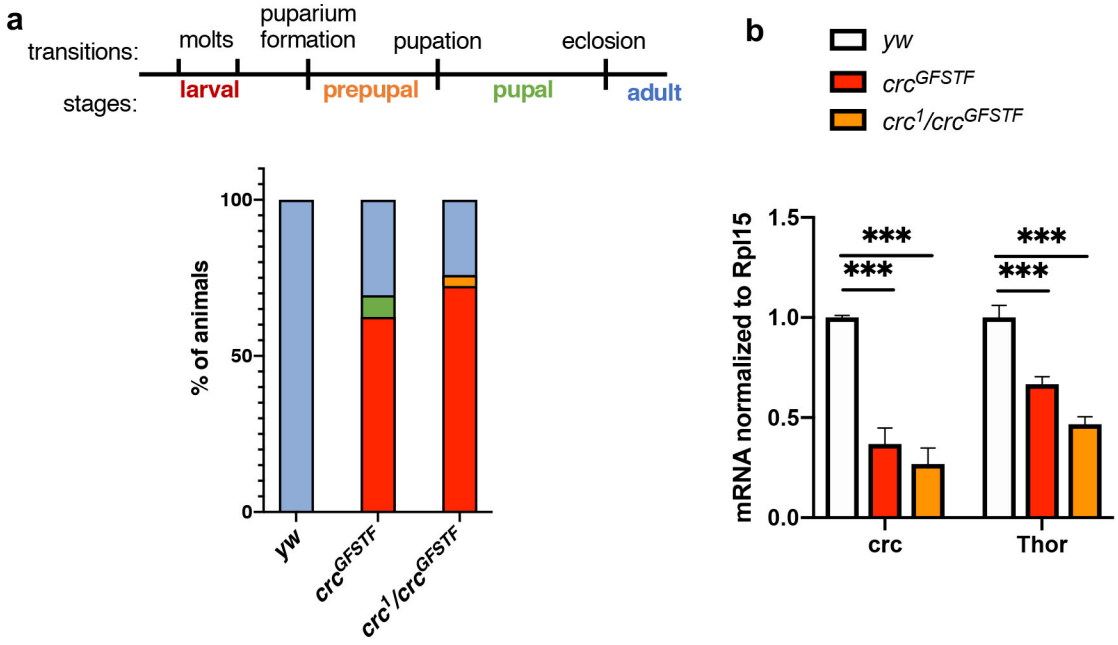

Fig. 3. *crc*^{GFSTF} is a *crc* hypomorphic allele

a. (Top) Schematic showing transitions and stages during *Drosophila* development. (Bottom) Lethal phase analysis for control (*yw*), *crc*^{GFSTF} homozygotes, and transheterozygotes (*crc*^{GFSTF}/*crc*^{1}), color-coded per the schematic. n=100 for each genotype.

b. qPCR analysis of *crc* and its transcriptional target, *Thor*, normalized to *Rpl15* from wandering 3rd instar larval stages when crc expression is known to be elevated. Data represent the mean of 3 independent experiments, error bars represent standard error. ***= p<0.0001 calculated by a paired two-tailed *t*-test.

Figure 4

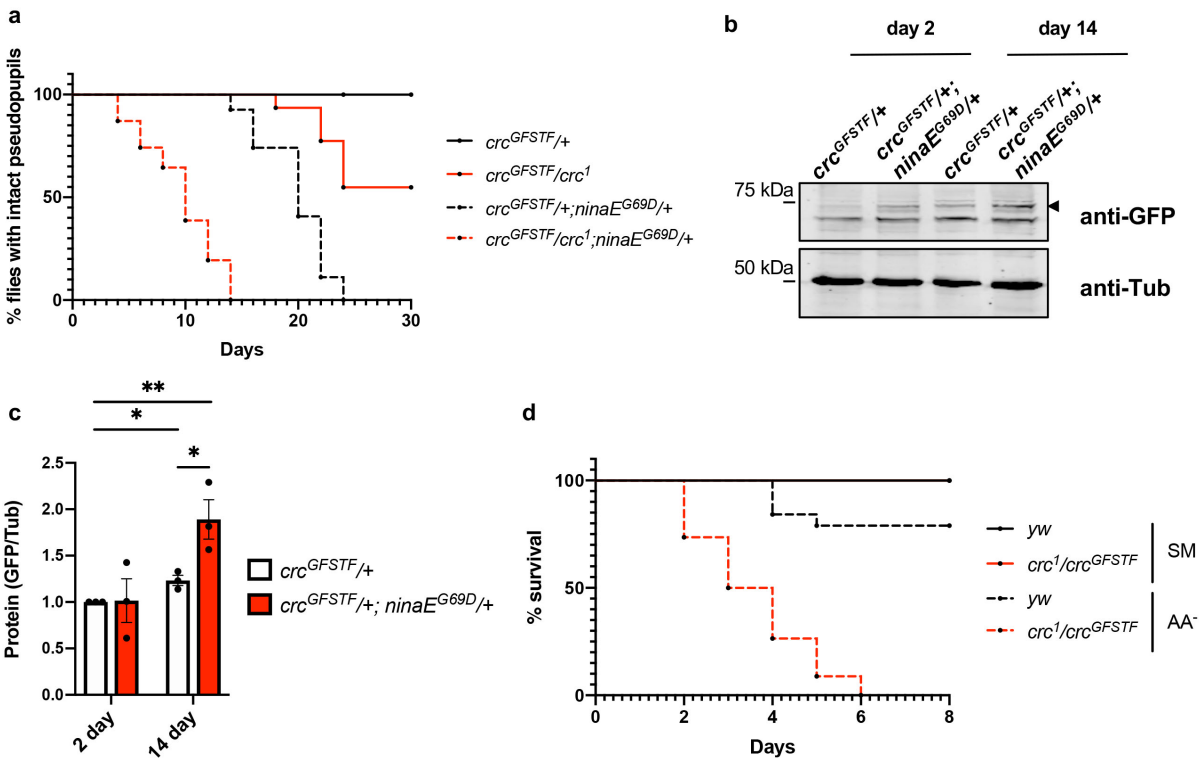

Fig. 4. crc mediates *Perk* and *Gcn2* phenotypes in adult animals

a. Time course of pseudopupil degeneration in control and $ninaE^{G69D}$/+ flies in *crc* heterozygote (crc^{GFSTF}/+) and transheterozygous mutants (crc^{GFSTF}/crc^{1}). The difference in the course of retinal degeneration between the following pairs is statistically significant as assessed by the Log-rank (Mantel-Cox) test ($p < 0.001$): crc^{GFSTF}/+ and crc^{GFSTF}/+;$ninaE^{G69D}$/+, crc^{GFSTF}/crc^{1} and crc^{GFSTF}/crc^{1};$ninaE^{G69D}$/+, and, crc^{GFSTF}/+ and crc^{GFSTF}/crc^{1}. (n = 100).

b. Western blot analysis of fly head extracts from young (1-2 day) and aged (14-16 day) old flies of the control and $ninaE^{G69D}$/+ animals also heterozygous for crc^{GFSTF}. The upper panel shows the blot probed with anti-GFP to detect the crc-GFP fusion protein (distinguished by the black arrowhead) and lower panel shows Tubulin (anti-Tub) as a

614 loading control.

615 c. Quantification of western blotting data in (b) showing crc-GFP normalized to Tubulin.
616 Data represent the mean from three independent experiments, error bars represent
617 standard error. **= p<0.001, *=p<0.01 calculated by a paired two-tailed *t*-test.

618 d. Time course of survival rate of adult females of indicated genotypes when fed with
619 standard media (SM, solid lines) or amino acid deprived media (AA^-, broken lines). Note
620 that the curves for the flies fed SM for *yw* (solid black) and crc^{GFSTF}/crc (solid red) overlap
621 entirely. The difference in the survival rates between the following pairs is statistically
622 significant as assessed by the Log-rank (Mantel-Cox) test ($p < 0.001$): *yw* (SM) and *yw*
623 (AA^-), crc^{GFSTF}/crc (SM) and crc^{GFSTF}/crc (AA^-), *yw* (AA^-) and crc^{GFSTF}/crc (AA^-). ($n = 100$).

624

625

626

Figure 5

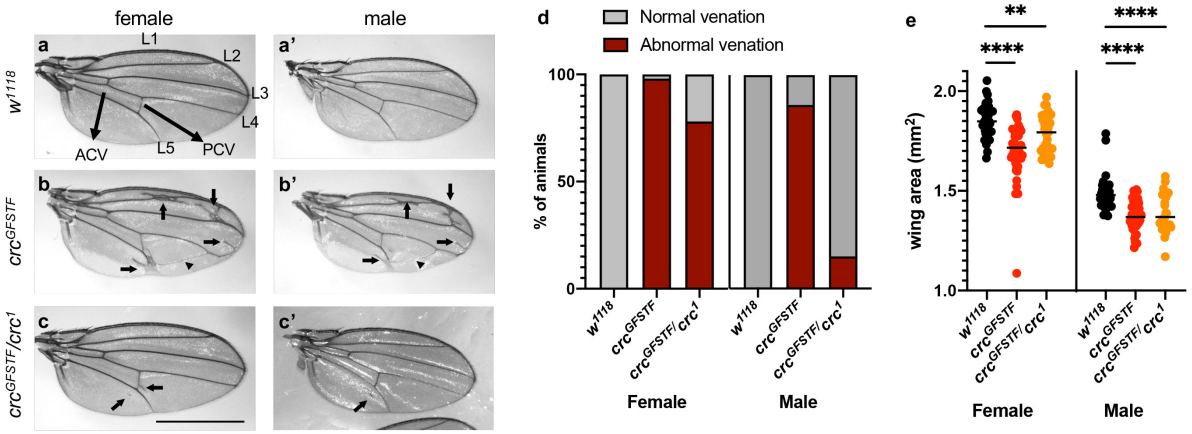

Fig. 5. Adult *crc* mutants display developmental defects in the wing

a-c. Grayscale images of the right wing from female (a-c) or male (a'-c') flies from the indicated genotypes. (a) shows the arrangement of wing veins in control (w^{1118}) flies with L1-L5 marking longitudinal veins, and arrows marking the anterior cross vein (ACV) and posterior cross vein (ACV). Ectopic longitudinal veins in crc^{GFSTF} homozygotes and crc^{GFSTF}/crc^{1} transheterozygotes (b, b', c, c') are marked by arrows and arrow heads point to ectopic cross veins. Scale bar= 1000μm.

d. The penetrance of the ectopic vein phenotype in (a-c) quantified from 40 animals of each sex of the indicated genotypes.

e. Area of the right wing from male and female flies of the indicated genotypes as measured in ImageJ. n≥27 for each genotype. Data represent the mean and error bars represent standard error. **= p<0.001, ****= p<0.00001 calculated by an unpaired two-tailed *t*-test.

Figure 6

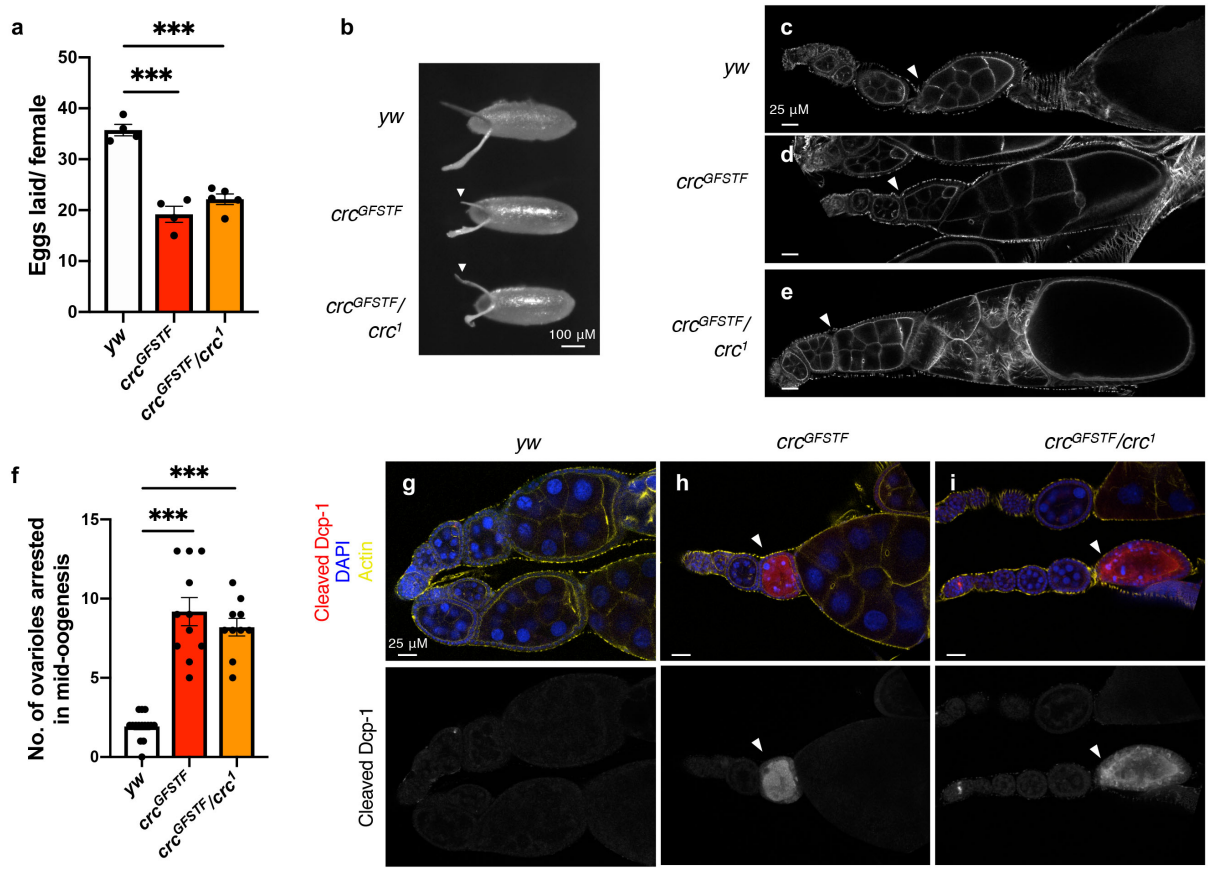

Fig. 6. *crc* mutant females show reduced fertility due to a block in oogenesis

a. Number of eggs laid per female in a 24-hour period for control (*yw*), and *crc* mutants. The data are the mean from 4 independent experiments with five females per experiment, error bars represent standard error. ***= p<0.0001, calculated by a paired two-tailed *t*-test.

b. Grayscale images of 0-24 hour eggs from females of the indicated genotypes. White arrowheads indicate dorsal appendage defects in eggs laid by *crc* mutant females, in comparison to well-formed and elongated dorsal appendages in eggs laid by control females (*yw*).

c-e. Confocal images of individual ovarioles from indicated genotypes, counterstained

654 with phalloidin (actin). Control ovarioles (*yw*) show clearly delineated individual egg
655 chambers (white arrowheads, c) that are appropriately sized for each stage. *crc* mutant
656 ovarioles (crc^{GFSTF}, crc^{GFSTF}/crc^{1}) show enlarged stage 10 egg chambers, with no clear
657 delineation between individual egg chambers (white arrowheads, d-e) indicating a block
658 in oogenesis.
659 f. The number of ovarioles per ovary showing enlarged stage 10 egg chambers, which
660 are indicative of a mid-oogenesis arrest. Data represent the mean from individual ovaries
661 of 11 animals, error bars represent standard error. ***= $p<0.0001$, calculated by an
662 unpaired two-tailed *t*-test.
663 g-i. Confocal images of ovaries from the indicated genotypes stained with the cell death
664 marker cleaved Dcp-1 (red), nuclei counterstained with DAPI (blue) and phalloidin
665 marking actin (yellow). White arrowheads point to egg chambers in *crc* mutant ovarioles
666 (crc^{GFSTF}, crc^{GFSTF}/crc^{1}) that show elevated Dcp-1 staining.